J|A|C|S ARTICLES

Published on Web 08/05/2009

Counterion-Dependent Valence Tautomerization of Ferrocenyl-Conjugated Pyrylium Salts

Mio Kondo,[†] Maai Uchikawa,[†] Kosuke Namiki,[†] Wen-Wei Zhang,[†] Shoko Kume,[†] Eiji Nishibori,[‡] Hiroyuki Suwa,[‡] Shinobu Aoyagi,[‡] Makoto Sakata,[‡] Masaki Murata,[†] Yoshio Kobayashi,[§] and Hiroshi Nishihara*[,†]

Department of Chemistry, School of Science, The University of Tokyo, 7-3-1 Hongo, Bunkyo-ku, Tokyo 113-0033, Japan, Department of Applied Physics, Nagoya University, Nagoya 464-8603, Japan, and The Institute for Physical and Chemical Research (RIKEN), Hirosawa, Wako, Saitama, Japan

Received January 18, 2009; E-mail: nisihara@chem.s.u-tokyo.ac.jp

Abstract: 1-Ferrocenylethynylanthraquinone **(1-FcAq)**, which is a donor (D)−acceptor (A) conjugated compound consisting of a ferrocene (Fc) acting as a donor, an anthraquinone (Aq) acting as an acceptor, and an ethynyl linker, undergoes a cyclocondensation reaction with strong organic acid, and forms 2-ferrocenyloxodihydrodibenzochromenylium salts (**[1-FcPyl]$^+$X$^-$** where X = TFSI, TfO, PF_6, and BF_4). **[1-FcPyl]$^+$** were also characterized as conjugated donor−acceptor compounds, and electrochemical properties, UV−vis absorption spectra, single-crystal X-ray analysis, and TD-DFT calculations have indicated that the LUMO level of **[1-FcPyl]$^+$** is lower than that of **1-FcAq** because of the much larger π-conjugated system in **[1-FcPyl]$^+$**. Variable-temperature Mössbauer spectroscopy (12−300 K) showed that Fe(II) was dominant for the $TFSI^-$, PF_6^-, and BF_4^- salts of **[1-FcPyl]$^+$**; although the Fe(III) species was also observed at all temperature ranges, the molar ratio of Fe(III) species increased at higher temperatures in the $TFSI^-$ and PF_6^- salts. This finding indicates that valence tautomerization (VT) between **1-FcPyl$^+$** and **1-Fc$^+$Pyl** occurs in the solid state of the $TFSI^-$ and the PF_6^- salts, but not in the BF_4^- salt. Variable-temperature (3.5−310 K) IR spectroscopy showed that the frequencies of the skeletal vibration of the ferrocene moiety decreased with increasing temperature in the $TFSI^-$ and PF_6^- salts, indicating the development of a ferrocenium-like character. The precision of the bond lengths of the **[1-FcPyl]$^+$** moiety (0.003−0.004 Å) determined by single-crystal X-ray analysis (113 and 273 K) is not sufficient to demonstrate the effect of the counterion on VT. The dihedral angle between the ferrocene and the pyrylium moieties in the BF_4^- salt (11.25(15)°) is larger than that in the $TFSI^-$ (6.63(12)°) and PF_6^- (9.55(15)°) salts. Furthermore, the planarity of the acceptor moiety (estimated from the dihedral angle between Ph1 and Ph2) is lower in the BF_4^- salt compared with that of other salts. These increased dihedral angles might cause a weaker D−A interaction and a destabilization of the acceptor moiety (i.e., raising a LUMO level), leading to lower stability of the Fe(III) (**1-Fc$^+$Pyl**) species. Variable-temperature X-ray powder diffraction (VT XRPD, 100−300 K) revealed that the temperature dependence of the Fe−P distance in the PF_6^- salt was smaller than that of the Fe−B distance in the BF_4^- salt. Our interpretation of this phenomenon is that the molar ratio of the Fe(III) species is increased in the PF_6^- salt, and that the Coulombic force between the ferrocene moiety and PF_6^- anion increases, preventing an increase in the Fe−P distance. This indicates that the electrostatic interaction between the **[1-FcPyl]$^+$** moiety and the counteranion may affect the occurrence of VT.

Introduction

A number of molecules that change their electronic structure in response to external stimuli such as light, protons, and temperature have been developed in recent decades.[1] Since the electronic structure of a molecule directly influences its physical properties, these switching materials are promising candidates for inclusion in molecular devices.[2] Among molecules with switching properties are those that exhibit the phenomenon of valence tautomerization (VT),[3] which involves reversible intramolecular electron transfer between two redox-active sites. Furthermore, the combination of donor (D) and acceptor (A) molecules is a promising way to incorporate unique functional properties; D and A readily interact both inter- and intramolecularly to generate new electronic states and display physical properties that cannot be achieved by the donor or acceptor alone.[4−7] Therefore, the introduction of a switching moiety into a D−A system is expected to give rise to a novel class of materials.

In this context, we studied the chemistry of a new class of a donor−acceptor π-conjugated complex, 1-ferrocenylethynylanthraquinone (**1-FcAq**), which may be expected to change their intramolecular D−A interaction upon protonation.[8−10] In our previous communication on the protonation behavior of **1-FcAq**,[10] we revealed that **1-FcAq** reacted with a strong organic acid, trifluoromethanesulfoneimide (TFSIH), to produce a tetracyclic compound, **[1-FcPyl]$^+$TFSI$^-$** (Scheme 1), which

[†] The University of Tokyo.
[‡] Nagoya University.
[§] The Institute for Physical and Chemical Research (RIKEN).

 10.1021/ja900393e CCC: $40.75

exhibited VT between **1-Fc$^+$Pyl** and **1-FcPyl**$^+$ in the crystalline state (Scheme 2). The cyclocondensation reaction of **1-FcAq** applies generally to various 1-arylethynylanthraquinone derivatives; Scheme 3 shows the conversion of **1-RAq** to **[1-RPyl]**$^+$, where **R** = phenyl (Ph), *m*-tolyl (*m*-Tol), and *p*-tolyl (*p*-Tol).[10] From the result of UV−vis absorption measurement and TD-DFT calculation, it is suggested that the LUMO level of **1-FcAq** and **1-RAq** is drastically lowered upon cyclization reaction to **[1-FcPyl]**$^+$ and **[1-RPyl]**$^+$'s. Therefore, we propose that the ethynylanthraquinone moiety could be utilized as a proton-responsive switch that modifies the LUMO level of molecules. It is also important that **[1-FcPyl]**$^+$ and **[1-RPyl]**$^+$ are cationic species: in the crystalline state, the anionic counterion is an important factor in determining packing structures and the strength of intermolecular interactions, which affect the conformation and electronic structure of the host cationic species. Therefore, we expected that VT in **1-FcPyl**$^+$ could be controlled by changing the counterion.

Scheme 1. Cyclocondensation Reaction of **1-FcAq**

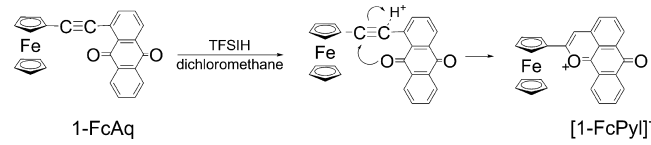

Scheme 2. Valence Tautomerism of **[1-FcPyl]**$^+$

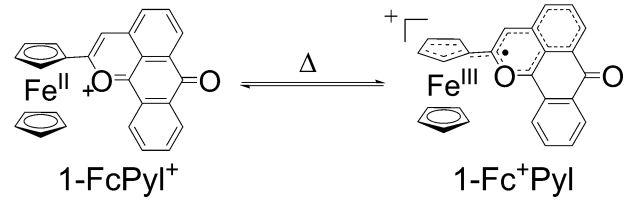

Scheme 3. Cyclocondensation Reaction of **1-RAq**

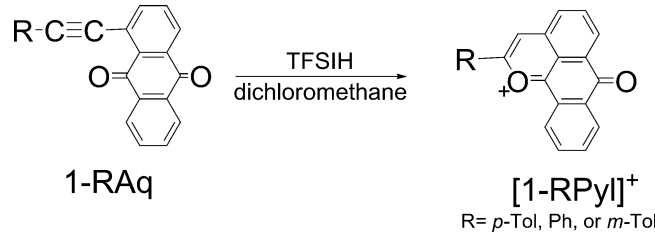

In this contribution, we report the switching of VT properties of **[1-FcPyl]**$^+$ with the perturbation of counteranions. We prepared several salts of **[1-FcPyl]**$^+$ with different counterions, **[1-FcPyl]$^+$X$^-$** (**X** = **TFSI**, **TfO**, **BF$_4$**, and **PF$_6$**), and studied their physical properties both in solution and in the crystalline state. TFSI$^-$ and PF$_6^-$ salts exhibited VT phenomena between **1-FcPyl**$^+$ and **1-Fc$^+$Pyl** in the crystalline state, although all salts in solution and BF$_4^-$ salt in the crystalline phase were in **1-FcPyl**$^+$ state at room temperature. The effect of counteranions on the VT phenomena of **[1-FcPyl]**$^+$ is reported in detail.

Results

Reactivity of 1-FcAq with Organic Acids. The cyclocondensation reaction of **1-FcAq** was performed using the acids trifluoromethanesulfoneimide (TFSIH), trifluoromethanesulfonic acid (TfOH, pK_a = ca. −15), and trifluoroacetic acid (TFA, pK_a = −0.25) as proton sources. According to studies in the

(1) (a) Irie, M. *Chem. Rev.* **2000**, *100*, 1685–1716. (b) Rowan, S. J.; Cantrill, S. J.; Cousins, G. R. L.; Sanders, J. K. M.; Stoddart, J. F. *Angew. Chem., Int. Ed.* **2002**, *41*, 898–952. (c) Kume, S.; Murata, M.; Ozeki, T.; Nishihara, H. *J. Am. Chem. Soc.* **2005**, *127*, 490–491. (d) Sakamoto, R.; Murata, M.; Kume, S.; Sampei, S.; Sugimoto, M.; Nishihara, H. *Chem. Comm.* **2005**, 1215–1217. (e) Sato, O.; Tao, J.; Zhang, Y.-Z. *Angew. Chem., Int. Ed.* **2007**, *46*, 2152–2187. (f) Champin, B.; Mobian, P.; Sauvage, J.-P. *Chem. Soc. Rev.* **2007**, *36*, 358–366. (g) Muratsugu, S.; Kume, S.; Nishihara, H. *J. Am. Chem. Soc.* **2008**, *130*, 7204–7205. (h) Arai, R.; Uemura, S.; Irie, M.; Matsuda, K. *J. Am. Chem. Soc.* **2008**, *130*, 9371–9379. (i) Duriska, M. B.; Neville, S. M.; Moubaraki, Cashion, B. J. D.; Halder, G. J.; Chapman, K. W.; Balde, C.; Létard, J.-F.; Murray, K. S.; Kepert, C. J.; Batten, S. R. *Angew. Chem., Int. Ed.* **2009**, *48*, 2549–2552.

(2) (a) Joachim, C.; Gimzewski, J. K.; Aviram, A. *Nature* **2000**, *408*, 541–548. (b) Seminario, J. M. *Nat. Mater.* **2005**, *4*, 111–113. (c) Green, J. E.; Choi, J. W.; Boukai, A.; Bunimovich, Y.; Halperin, E. J.; DeIonno, E.; Luo, Y.; Sheriff, B. A.; Xu, K.; Shin, Y. S.; Tseng, H.-R.; Stoddart, J. F.; Heath, J. R. *Nature* **2007**, *445*, 414–417. (d) Mativetsky, J. M.; Pace, G.; Elbing, M.; Rampi, M. A.; Mayor, M.; Samorì, P. *J. Am. Chem. Soc.* **2008**, *130*, 9192–9193. (e) Klajn, R.; Fang, L.; Coskun, A.; Olson, M. A.; Wesson, P. J.; Stoddart, J. F.; Grzybowski, B. A. *J. Am. Chem. Soc.* **2009**, *131*, 4233–4235.

(3) (a) Tao, J.; Maruyama, H.; Sato, O. *J. Am. Chem. Soc.* **2006**, *128*, 1790–1791. (b) Mochida, T.; Takazawa, K.; Matsui, H.; Takahashi, M.; Takeda, M.; Sato, M.; Nishio, Y.; Kajita, K.; Mori, H. *Inorg. Chem.* **2005**, *44*, 8628–8641. (c) Salamon, S. B.; Brewer, S. H.; Depperman, E. C.; Franzen, S.; Kampf, J. W.; Kirk, M. L.; Kumar, R. K.; Lappi, S.; Peariso, K.; Preuss, K. E.; Shultz, D. A. *Inorg. Chem.* **2006**, *45*, 4461–4467. (d) Hearns, N. G. R.; Korcők, J. L.; Paquette, M. M.; Preuss, K. E. *Inorg. Chem.* **2006**, *45*, 8817–8819. (e) Rotthaus, O.; Thomas, F.; Jarjayes, O.; Philouze, C.; Saint-Aman, E.; Pierre, J.-L. *Chem.—Eur. J.* **2006**, *12*, 6953–6962. (f) Naumov, P.; Belik, A. A. *Inorg. Chem. Commun.* **2008**, *11*, 465–469. (g) Kiriya, D.; Chang, H.-C.; Nakamura, K.; Tanaka, D.; Yoneda, K.; Kitagawa, S. *Chem. Mater.* **2009**, *21*, 1980–1988. (h) Diallo, A. K.; Daran, J.-C.; Varret, F.; Ruiz, J.; Astruc, D. *Angew. Chem., Int. Ed.* **2009**, *48*, 3141–3145.

(4) (a) Matsumoto, T.; Kominami, T.; Ueda, K.; Sugimoto, T.; Tada, T.; Noguchi, S.; Yoshino, H.; Murata, K.; Shiro, M.; Negishi, E.; Toyota, N.; Endo, S.; Takahashi, K. *Inorg. Chem.* **2002**, *41*, 4763–4769. (b) Alberola, A.; Coronado, E.; Galán-Mascarós, J. R.; Giménez-Saiz, C.; Gómez-García, C. J. *J. Am. Chem. Soc.* **2003**, *125*, 10774–10775. (c) Mukai, K.; Jinno, S.; Shimobe, Y.; Azuma, N.; Taniguchi, M.; Misaki, Y.; Tanaka, K.; Inoue, K.; Hosokoshi, Y. *J. Mater. Chem.* **2003**, *13*, 1614–1621. (d) Wang, G.; Slebodnick, C.; Butcher, R. J.; Tam, M. C.; Crawford, T. D.; Yee, G. T. *J. Am. Chem. Soc.* **2004**, *126*, 16890–16895. (e) Nakajima, H.; Katsuhara, M.; Ashizawa, M.; Kawamoto, T.; Mori, T. *Inorg. Chem.* **2004**, *43*, 6075–6082.

(5) (a) Nishihara, H.; Kurashina, M.; Aramaki, K.; Kubo, K. *Synth. Met.* **1999**, *101*, 457–458. (b) Chollet, M.; Guerin, L.; Uchida, N.; Fukaya, S.; Shimoda, H.; Ishikawa, T.; Matsuda, K.; Hasegawa, T.; Ota, A.; Yamochi, H.; Saito, G.; Tazaki, R.; Adachi, S.; Koshihara, S. *Science* **2005**, *307*, 86–89.

(6) (a) Ferraris, J.; Cowan, D. O.; Walatka, V.; Perlstein, J. H., Jr. *J. Am. Chem. Soc.* **1973**, *95*, 948–949. (b) Saito, G.; Sasaki, H.; Aoki, T.; Yoshida, Y.; Otsuka, A.; Yamochi, H.; Drozdova, O. O.; Yakushi, K.; Kitagawa, H.; Mitani, T. *J. Mater. Chem.* **2002**, *12*, 1640–1649.

(7) (a) Ratera, I.; Molina, D. R.; Renz, F.; Ensling, J.; Wurst, K.; Rovira, C.; Gütlich, P.; Veciana, J. *J. Am. Chem. Soc.* **2003**, *125*, 1463–1464. (b) Ratera, I.; Sporer, C.; Ruiz-Molina, D.; Ventosa, N.; Baggerman, J.; Brouwer, A. M.; Rovira, C.; Veciana, J. *J. Am. Chem. Soc.* **2007**, *129*, 6117–6129. (c) D'Avino, G.; Grisanti, L.; Guasch, J.; Ratera, I.; Veciana, J.; Painelli, A. *J. Am. Chem. Soc.* **2008**, *130*, 12064–12072. (d) Sporer, C.; Ratera, I.; Ruiz-Molina, D.; Gancedo, J. V.; Ventosa, N.; Wurst, K.; Jaitner, P.; Rovira, C.; Veciana, J. *Solid State Sci.* **2009**, *11*, 786–792.

(8) Murata, M.; Fujita, T.; Yamada, M.; Kurihara, M.; Nishihara, H. *Chem. Lett.* **2000**, 1328–1329.

(9) (a) Murata, M.; Yamada, M.; Fujita, T.; Kojima, K.; Kurihara, M.; Kubo, K.; Kobayashi, Y.; Nishihara, H. *J. Am. Chem. Soc.* **2001**, *123*, 12903–12904. (b) Nishihara, H.; Murata, M. *J. Inorg. Organomet. Polym. Mater.* **2005**, *15*, 147–156. (c) Kondo, M.; Murata, M.; Nishihara, H.; Nishibori, E.; Aoyagi, S.; Yoshida, M.; Kinoshita, Y.; Sakata, M. *Angew. Chem., Int. Ed.* **2006**, *45*, 5461–5464. (d) Kojima, K.; Zhang, W.-W.; Kondo, M.; Uchikawa, M.; Namiki, K.; Fujita, T.; Murata, M.; Kobayashi, Y.; Nishihara, H. *J. Inorg. Organomet. Polym. Mater.* **2007**, *17*, 135–141.

(10) Kondo, M.; Uchikawa, M.; Zhang, W.-W.; Namiki, K.; Kume, S.; Murata, M.; Kobayashi, Y.; Nishihara, H. *Angew. Chem., Int. Ed.* **2007**, *46*, 6271–6274.

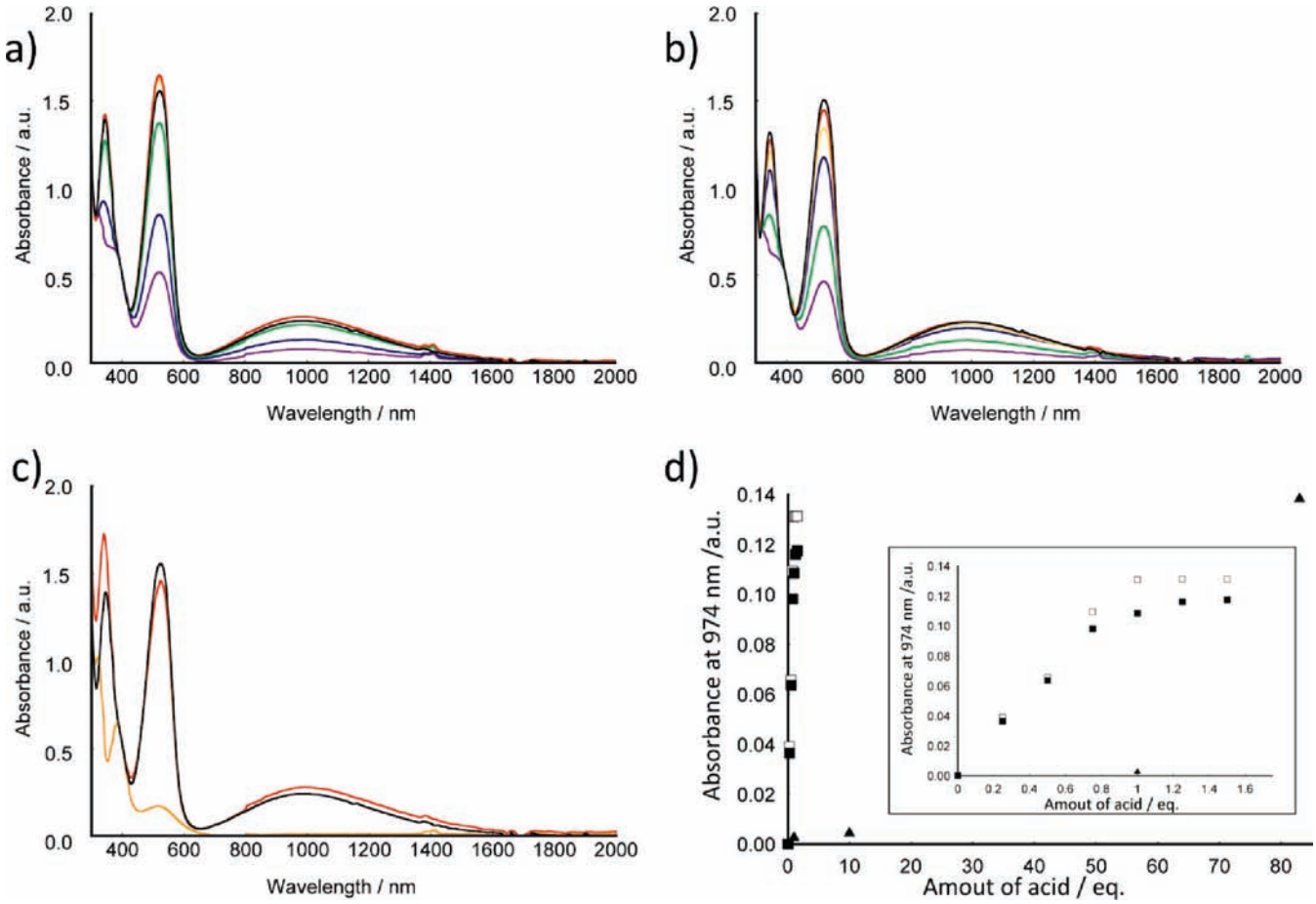

Figure 1. (a) UV−vis−NIR spectra of 0.5 mM **1-FcAq** upon addition of TFSIH (0.25 equiv (purple line), 0.50 equiv (blue line), 0.75 equiv (green line), 1.00 equiv (yellow line) 1.25 equiv (orange line), and 1.50 equiv (red line)), and that of 0.5 mM **[1-FcPyl]$^+$TFSI$^-$** (black line) in dichloromethane. (b) UV−vis−NIR spectra of 0.5 mM **1-FcAq** upon addition of TfOH (0.25 equiv (purple line), 0.50 equiv (blue line), 0.75 equiv (green line), 1.00 equiv (yellow line) 1.25 equiv (orange line), and 1.50 equiv (red line)) and that of 0.5 mM **[1-FcPyl]$^+$TFSI$^-$** (black line) in dichloromethane. (c) UV−vis−NIR spectra of 0.5 mM **1-FcAq** upon addition of TFA (1.00 equiv (yellow line), 10.0 equiv (orange line) and 83 equiv (red line)) and that of 0.5 mM **[1-FcPyl]$^+$TFSI$^-$** (black line) in dichloromethane. (d) Change of absorbance at 974 nm upon addition of TFSIH (open squares), TfOH (squares), and TFA (triangles). (Inset) Enlarged plot of 0.00−1.75 equiv.

gaseous phase, TFSIH is a stronger acid than TfOH,[11] giving the following order of acidity: TFSIH > TfOH > TFA. Each acid was added stepwise to a 5.0 mM solution of **1-FcAq** in dichloromethane, and the change in the absorption spectrum of a 10-fold diluted sample was recorded (Figure 1). With TFSIH and TfOH, the spectral changes gave an isosbestic point, and 1.0−1.25 equiv of acid were required to give a spectrum consistent with that of **[1-FcPyl]$^+$TFSI$^-$** in dichloromethane (*vide infra*). These results suggest that **1-FcAq** was converted almost quantitatively to **[1-FcPyl]$^+$** by TFSIH and TfOH. In contrast, more than 80 equiv of the weaker acid TFA were needed to complete the conversion of **1-FcAq** to **[1-FcPyl]$^+$**; the spectral changes gave an isosbestic point (Figure S1), suggesting the absence of a side reaction. Thus the protonated form of **1-FcAq**, the amount of which is dependent on the acidity of the proton source, cyclized quantitatively to give **[1-FcPyl]$^+$**.

Syntheses and Characterization of [1-FcPyl]$^+$X$^-$ (X = TFSI, TfO, BF$_4$, and PF$_6$). Two methods were used to synthesize **[1-FcPyl]$^+$X$^-$**, the protonated form of **1-FcAq** with various counterions. The first method comprised direct reaction of **1-FcAq** with the acid TFSIH or TfOH to form **[1-FcPyl]$^+$TFSI$^-$** or **[1-FcPyl]$^+$TfO$^-$**, respectively. **[1-FcPyl]$^+$TFSI$^-$** was synthesized by adding 1.7 equiv of TFSIH to a dichloromethane solution of **1-FcAq**, giving an isolated yield of up to 82%. The air-stable product was soluble in acetonitrile and benzonitrile, and less so in dichloromethane, 1,2-dichloroethane, and chloroform. **[1-FcPyl]$^+$TfO$^-$** was synthesized by the reaction of **1-FcAq** with 3.2 equiv of TfOH, giving an isolated yield of 95%. The product was rather moisture-sensitive and soluble in polar organic aprotic solvents such as acetonitrile, benzonitrile, dichloromethane, 1,2-dichloroethane, and chloroform.

In the second method, TfO$^-$ was exchanged with other anions. **[1-FcPyl]$^+$PF$_6^-$** and **[1-FcPyl]$^+$BF$_4^-$** were synthesized by adding an excess of tetrabutylammonium tetrafluoroborate or hexafluorophosphate to a saturated solution of **[1-FcPyl]$^+$TfO$^-$** in dichloromethane. The salts **[1-FcPyl]$^+$PF$_6^-$** and **[1-FcPyl]$^+$BF$_4^-$** were isolated by filtration, as they were less soluble in dichloromethane than **[1-FcPyl]$^+$TfO$^-$**. **[1-FcPyl]$^+$PF$_6^-$** and **[1-FcPyl]$^+$BF$_4^-$** were stable in air, soluble in acetonitrile and benzonitrile, and less soluble in dichloromethane, 1,2-dichloroethane, and chloroform. The four **[1-FcPyl]$^+$** salts synthesized by the above two methods were characterized by ^{1}H NMR and elemental analyses, and molecular structures of the TFSI$^-$, BF$_4^-$,

(11) (a) Koppel, I. A.; Taft, R. W.; Anvia, F.; Zbu, S.-Z.; Hu, L.-Q.; Sung, K.-S.; DesMarteau, D. D.; Yagupolskii, L. M.; Yagupolskii, Y. L.; Ignat'ev, N. V.; Kondratenko, N. V.; Volkonskii, A. Y.; Vlasov, V. M.; Notario, R.; Maria, P.-C. *J. Am. Chem. Soc.* **1994**, *116*, 3047–3057. (b) Favier, I.; Duñach, E. *Tetrahedron Lett.* **2004**, *45*, 3393–3395.

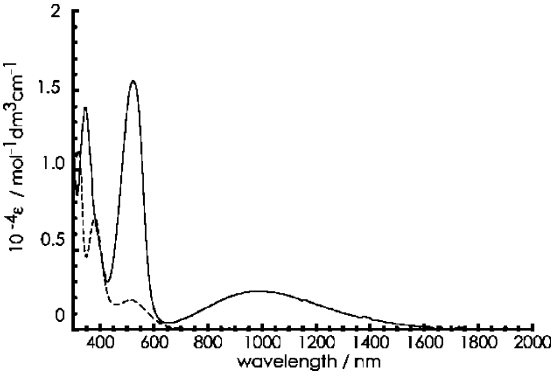

Figure 2. UV−vis−NIR absorption spectra of **[1-FcPyl]$^+$TFSI$^-$** (solid line) and **1-FcAq** (dashed line) in dichloromethane.

and PF_6^- salts were determined by single-crystal X-ray crystallography.

Electronic Structure of [1-FcPyl]$^+$ Salts in Solution. The UV−vis−NIR spectra of **[1-FcPyl]$^+$X$^-$** (X = TFSI, TfO, PF_6, and BF_4) and **1-FcAq** in dichloromethane are shown in Figures 2 and S2. Spectra of **[1-FcPyl]$^+$X$^-$** contained two new bands absent in the **1-FcAq** spectrum: one in the visible region at λ_{max} = 522 nm (ε_{max} = 1.51−1.57 × 10^4 M^{-1} cm^{-1}) and the other in the near-IR region at λ_{max} = 974−976 nm (ε_{max} = 2.3−2.5 × 10^3 M^{-1} cm^{-1}). There were no counterion effects on the electronic structure of **[1-FcPyl]$^+$** in solution, as evidenced by ^{1}H NMR (Figure S3).

The electronic structure of **[1-FcPyl]$^+$** was calculated by the TD-DFT method using B3LYP/LanL2DZ basis sets. The molecular orbitals, and experimental and calculated excitation energies to the lowest excited state of **[1-FcPyl]$^+$** are shown in Figure 3 and Table S1, respectively. The band in the region of 520 nm was assigned mainly to the $\pi-\pi^*$ transition from HOMO−2 (100), consisting mostly of a π orbital in the ferrocene moiety, to LUMO (103), comprising a π^* orbital in the dibenzochromenylium moiety. The band observed in the near-IR region (λ_{max} = 959 nm) was assignable to the intervalence charge transfer (IVCT) transition from HOMO (102), consisting of the $d_{x^2-y^2}$ π orbital of the ferrocene moiety, to LUMO (103). The character of the band was also indicated by absorption measurement of **[1-FcPyl]$^+$** in various solvents. As shown in Figure S4, the band exhibits negative solvatochromic behavior[12] (λ_{max} = 959 nm (in dichloromethane), 934 nm (in benzonitrile), and 878 nm (in acetonitrile)), suggesting the charge transfer character of the band.

Cyclic voltammograms of **1-FcAq** and **[1-FcPyl]$^+$** in Bu_4NClO_4/dichloromethane at 293 K and that of **1-FcAq** obtained upon stepwise addition of TfOH are respectively shown in a and c of Figure 4. **1-FcAq** showed reversible two-step 1e$^-$ reduction ascribed to the anthraquinone moiety[13] (−1.83 and −1.39 V vs ferrocenium/ferrocene (Fc^+/Fc)), and one-step oxidation ascribed to the ferrocene moiety (0.11 V vs Fc^+/Fc). Upon addition of TfOH, these three redox waves disappeared, and two new reversible redox waves were observed at −1.06 V, −0.31 V, and 0.30 V. By comparison with the cyclic voltammograms of **[1-*p*-TolPyl]$^+$TFSI$^-$** (Figure S5), the wave at −1.06 and −0.31 V can be assigned to the reduction of the dibenzopyrylium moiety, and the wave at 0.30 V to the oxidation of the ferrocene moiety. The difference between the first reduction potential and the first oxidation potential of **1-FcAq** and **[1-FcPyl]$^+$** was 1.50 and 0.61 V, respectively. This result suggests that the π^* (LUMO) level of **[1-FcPyl]$^+$** is lowered upon the cyclization reaction, resulting in a smaller HOMO−LUMO gap and bands in lower-energy region, and consistent with the UV−vis-NIR results and the TD-DFT calculation. The energy diagram of **[1-FcPyl]$^+$** compared with **1-FcAq** is depicted in Figure 4b.

In addition, the result that redox waves of the donor and the acceptor moiety were observed with relatively large potential separation ($\Delta E^{0'}$ = 0.61 V) clearly shows that electronic interaction between these moieties is not strong enough to cause VT state in solution.

The valence state of **[1-FcPyl]$^+$** was also determined by electrochemical measurement. The open circuit potential of **[1-FcPyl]$^+$** (0.06 V vs Fc^+/Fc) existed between the reduction potential of the pyrylium moiety and the oxidation potential of the ferrocene moiety. In the measurement using Bu_4NTFSI or Bu_4NBF_4 as electrolyte, the open circuit potentials of **[1-FcPyl]$^+$** were also located in the negative region to the redox potential of the ferrocene moiety. Therefore, it is suggested that all **[1-FcPyl]$^+$** salts have the Fe(II) form (**1-FcPyl$^+$** form) in solution at room temperature.

Molecular Structures of [1-FcPyl]$^+$ Salts. The molecular structures of **[1-FcPyl]$^+$X$^-$** (X = TFSI, PF_6, and BF_4) were determined by single-crystal X-ray crystallography. ORTEP drawings and crystallographic data measured at 113 K are shown in Figure 5a−c and Table 1, respectively. **[1-FcPyl]$^+$** has a pyrylium ring formed by the intramolecular cyclocondensation reaction between the ethynyl moiety and the carbonyl group in the anthraquinone moiety. Selected bond lengths in **[1-FcPyl]$^+$** and **1-FcAq** are shown in Tables 2 and S2. The lengths of C−C bonds in the pyrylium moiety (C11−C12−C13−C25−C26−O1) of the $TFSI^-$, PF_6^-, and BF_4^- salts of **[1-FcPyl]$^+$** are in the range of 1.366(4)−1.415(4) Å, 1.355(3)−1.422(4) Å, and 1.350(4)−1.415(5) Å, respectively. These results indicate that the pyrylium moiety of **[1-FcPyl]$^+$** has aromatic character. Variation in the bond lengths of the dibenzochromenylium moiety between the three salts were within the margin of error. The bond lengths of C24−C25 and C25−C26, which have single-bond character in **1-FcAq**, were shorter in **[1-FcPyl]$^+$** than in **1-FcAq**; furthermore, the bond length of C25−O1, which has double-bond character in **1-FcAq**, was longer in **[1-FcPyl]$^+$** than in **1-FcAq**. These changes in bond lengths suggest that the two π-conjugated systems of **1-FcAq**, which are separated at the carbonyl groups of the anthraquinone moiety, become united and expanded to the entire acceptor moiety upon cyclization to **[1-FcPyl]$^+$**. In other words, **[1-FcPyl]$^+$** has a larger π-conjugated system than **1-FcAq**, as predicted by the DFT calculation (*vide supra*).

Effect of Counterions on the VT Properties of [1-FcPyl]$^+$ in the Crystalline State: ^{57}Fe Mössbauer Spectra of [1-FcPyl]$^+$X$^-$ (X = TFSI, PF_6, and BF_4). Mössbauer spectra and the spectral parameters of **[1-FcPyl]$^+$X$^-$** (X = TFSI, PF_6, and BF_4) at various temperatures are shown in Figures 6 and S6−S8, and Table S3. In the case of the $TFSI^-$ salt, all spectra could be fit to two species, F1 and F2. F1 showed a quadrupole doublet with a splitting of 2.11(1)−2.10(1) mm s^{-1}, and an isomer shift of 0.53(1) mm s^{-1} at 12 K (Table S3). These values are typical for ferrocene derivatives.[14] F2 showed a quadrupole doublet

(12) Reichardt, C. *Chem. Rev.* **1994**, *94*, 2319.
(13) Chambers, J. Q. In *The Chemistry of the Quinonoid Compounds*; Patai, S., Ed., Chemistry of Functional Groups; Wiley-Interscience: New York, 1974; Chapter 14.
(14) Greenwood, N. N.; Gibb, T. C. *Mössbauer Spectroscopy*; Chapman and Hall Ltd.: London, 1971.

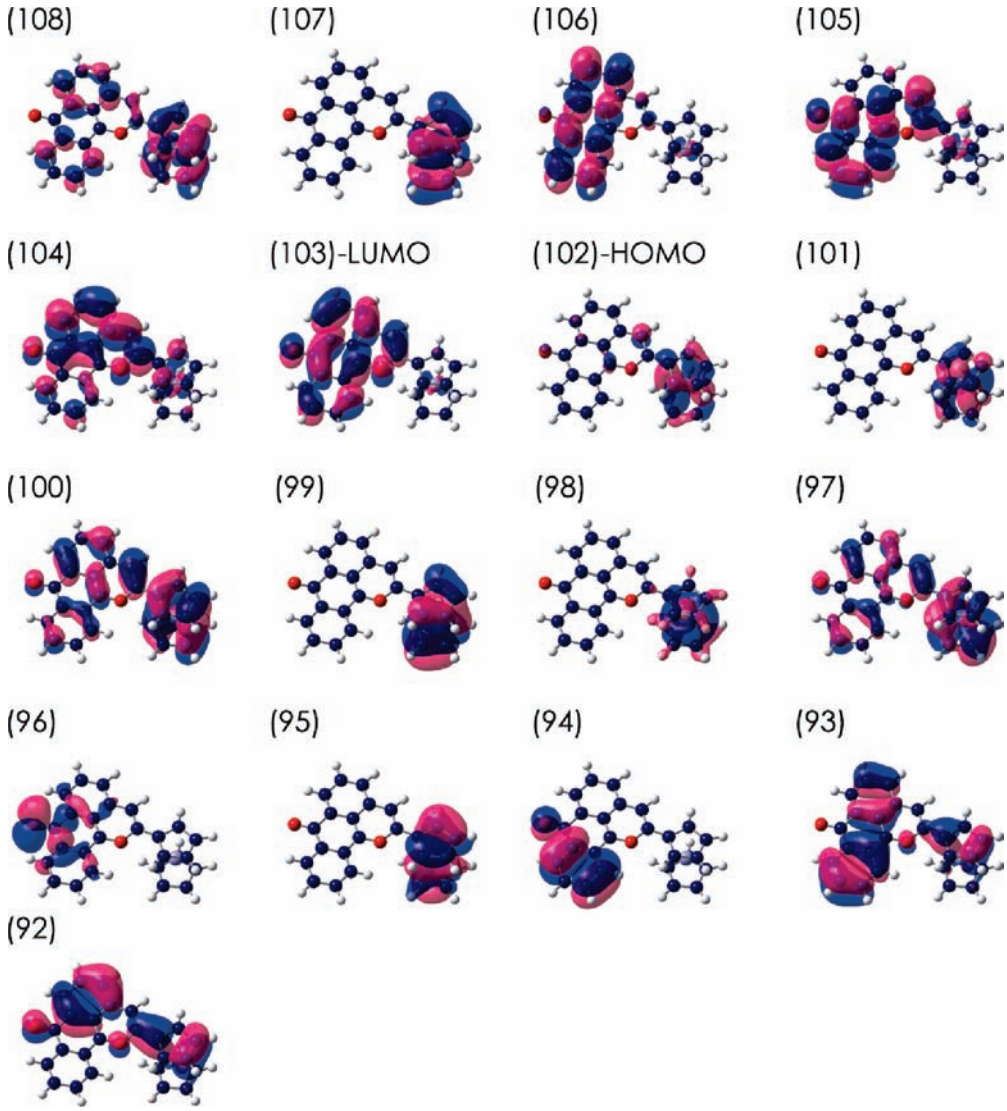

Figure 3. Molecular orbitals of **[1-FcPyl]**$^+$ calculated at the B3LYP/LanL2DZ level.

splitting of 0.54(1) mm s^{-1} at 12 K, which is characteristic of ferrocenium ions.[14] The isomer shift was 0.30(2) mm s^{-1}, which suggests a ferrocenium ion covalently linked to an acceptor molecule that shows VT properties.[7a] These data indicate that F1 and F2 can be assigned as the Fe(II) and Fe(III) species, respectively. The molar ratios of Fe(II) and Fe(III) (ϕ^{II} = Fe(II)/(Fe(II) + Fe(III)) and ϕ^{III} = Fe(III)/(Fe(II) + Fe(III)), respectively) were determined from the area fraction of F1 and F2 and are shown in Figure 6c. The ϕ^{III} value of the TFSI$^-$ salt showed a gradual and fully reversible rise as a function of temperature. This finding indicates that the change in temperature induces electron transfer from the iron center in ferrocene to the dibenzochromenylium moiety, as shown in Scheme 2. The energy difference between the Fe(II) and Fe(III) species ($\Delta E_{Fe(III)-Fe(II)}$) was determined from the ϕ^{III} values at various temperatures (Figure S9). The value of $\Delta E_{Fe(III)-Fe(II)}$ from 12 to 290 K was small (0.7 to -1.7 kJ mol^{-1}), indicating small enthalpy (ΔH) and entropy (ΔS) differences between the Fe(II) and Fe(III) states. Moreover, $\Delta E_{Fe(III)-Fe(II)}$ is estimated to be not constant at all temperature range, suggesting that the relative population of two species is not governed by the Boltzmann equation. In addition, the fact that the Fe(III) species was not observed in solution suggests that stabilization of the Fe(III) species or destabilization of the Fe(II) species occurred only in the crystalline state of **[1-FcPyl]$^+$TFSI$^-$** at the higher temperature region.

The existence of two species (F1 and F2) was also observed in the Mössbauer spectrum of the PF_6^- salt measured at 11 K. The isomer shift and quadrupole doublet splitting parameter of F1 were determined to be 0.539(2) mm s^{-1} and 2.238(3) mm s^{-1}, respectively. These values are almost the same as those observed for F1 in the TFSI$^-$ salt, allowing F1 to be assigned as the Fe(II) species. The quadrupole doublet splitting parameter of F2 varied significantly with temperature. At lower temperatures the low intensity of the Fe(II) peak prevented a satisfactory fit, causing overestimation of the area intensity. However, at higher temperatures the isomer shift and quadrupole splitting parameter of F2 in the PF_6^- salt were similar to those of F2 in the TFSI$^-$ salt. Moreover, the ϕ^{III} value in the PF_6^- salt showed a gradual and fully reversible increase as a function of temperature, similar to that observed in the TFSI$^-$ salt. Thus, F2 in the PF_6^- salt could be assigned as the Fe(III) species, and the results indicate that VT occurred in the PF_6^- salt in the same manner as in the TFSI$^-$ salt.

In contrast, the Mössbauer spectrum of the BF_4^- salt at 11 K fits to one species, F1. The isomer shift and quadrupole splitting

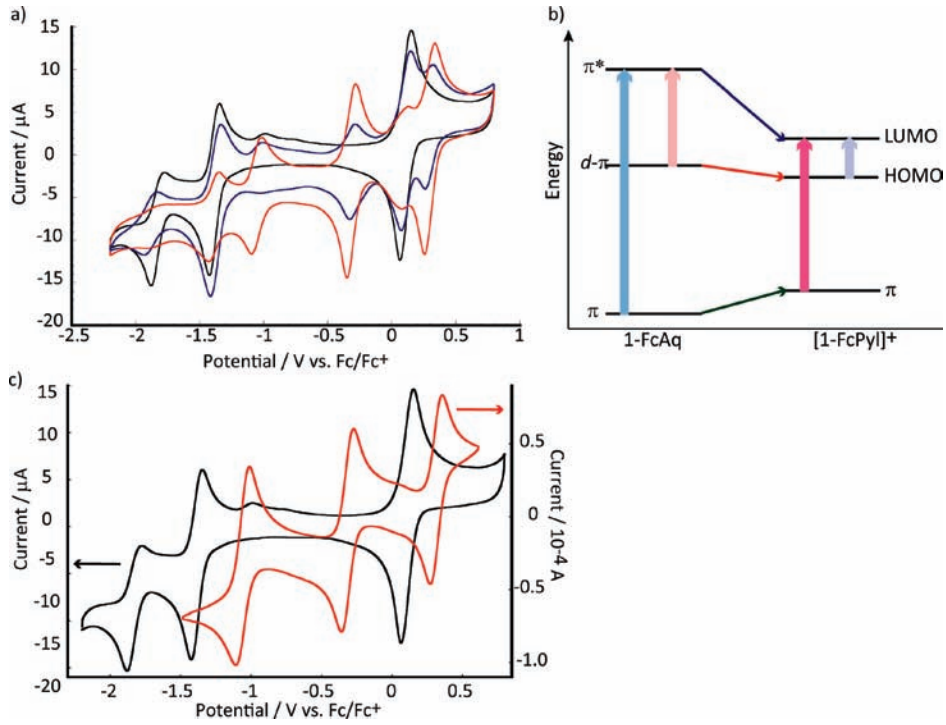

Figure 4. (a) Cyclic voltammograms of **1-FcAq** obtained at 293 K upon addition of 0.00 equiv (black line), 0.50 equiv (blue line), and 1.00 equiv (red line) of TfOH in 0.1 M Bu_4NClO_4−dichloromethane solution at 0.1 V s^{-1}. (b) Energy diagram of **[1-FcPyl]**$^+$ and **[1-FcPyl]** estimated from redox potentials and UV−vis−NIR absorption wavelengths. (c) Cyclic voltammograms of **1-FcAq** (black line) and **[1-FcPyl]**$^+$ (red line) in 0.1 M Bu_4NClO_4−dichloromethane at 0.1 V s^{-1}.

parameters of F1 were determined to be 0.544(2) mm s^{-1} and 2.238(3) mm s^{-1}, respectively. These values are in good agreement with those of F1 in the $TFSI^-$ and PF_6^- salts, allowing F1 in the BF_4^- salt to be assigned as the Fe(II) species. Unlike in the $TFSI^-$ and PF_6^- salts, VT was not observed in the BF_4^- salt.

The Effect of Counteranions on the Conformation and Packing Structure of [1-FcPyl]$^+$ in the Crystalline State. Figure 7 shows conformational differences in **[1-FcPyl]$^+$X$^-$** resulting from changes of anion, compared by adjusting the position of the Cp2 (C6−C10) moiety of **[1-FcPyl]$^+$BF$_4^-$** to that of **[1-FcPyl]$^+$TFSI$^-$** or **[1-FcPyl]$^+$PF$_6^-$**. The conformational changes of **1-FcPyl**$^+$ depending on the counteranions are estimated by comparing the changes of two dihedral angles, ϕ_1 and ϕ_2, where ϕ_1 is an angle between Cp2 (C6−C7−C8−C9−C10) and Pyl^+ (C11−C12−C13−C25−C26−O1) and ϕ_2 is an angle between Ph1 (C13−C14−C15−C16−C17−C26) and Ph2 (C19−C20−C21−C22−C23−C24), respectively. These two angles, ϕ_1 and ϕ_2, should reflect the π-conjugation between the donor and the acceptor moieties, and the distortion of the acceptor moiety, respectively. ϕ_1, showed some dependence on the anion; the angles were 6.63 (12)°, 9.55 (12)°, and 11.25 (15)° for the $TFSI^-$, PF_6^-, and BF_4^- salts, respectively. In the case of the BF_4^- salt, the size of the dihedral angle might result in a weaker D−A interaction, thus lowering the stability of the Fe(III) species and preventing VT (*vide supra*). To confirm this assumption, TD-DFT calculations with various ϕ_1 (0, 3, 6, 9, 12, 15 deg) were performed. As shown in Figure S10, the energy of IVCT band shifted to a higher-energy region with increasing ϕ_1. In other words, the electronic interaction through the π-conjugation between the donor and the acceptor moieties caused the smaller HOMO−LUMO gap of **[1-FcPyl]**$^+$. ϕ_2 exhibited large difference between the BF_4^- salt and other two salts; the angles were 4.06(12)°, 4,11(11)°, and 8.74(13)° for the $TFSI^-$, PF_6^-, and BF_4^- salts, respectively. The distorted acceptor moiety would lead to the rising of LUMO energy, and at last, prevent the electron transfer from the donor to the acceptor. From these two factors, the BF_4^- salt is less favorable to exhibit VT phenomena.

Figure 8 shows packing structures of the $TFSI^-$, PF_6^-, and BF_4^- salts. In the structure of the $TFSI^-$ salt, we observed $\pi-\pi$ stacking between the cyclopentadienyl ring of the ferrocene moiety and the benzopyrylium moiety. The average plane-to-plane distance between C6−C7−C8−C9−C10 and C11−C12−C13−C25−C26−O1 is 3.287(4) Å, indicating the existence of an intermolecular D−A interaction. The PF_6^- and BF_4^- salts had the same space group, $Pna2_1$, and the same packing structure. Unlike in the $TFSI^-$ salt, intermolecular interaction between the donor and acceptor moieties through $\pi-\pi$ stacking was not observed in the crystal structures of the PF_6^- and BF_4^- salts.

Diffuse Reflectance UV−vis−NIR Spectroscopy. The electronic structure of **[1-FcPyl]$^+$X$^-$** in the crystalline state was studied at room temperature by UV−vis−NIR spectroscopy. Figure 9 shows the diffuse reflectance UV−vis−NIR spectra of **[1-FcPyl]$^+$X$^-$** (X = TFSI, PF_6, and BF_4) dispersed to 1% w/w in KBr powder, and a UV−vis−NIR absorption spectrum of **[1-FcPyl]$^+$TFSI$^-$** in dichloromethane. Similar to the electronic spectra in solution, spectra of the salts in the crystalline state revealed a $\pi-\pi^*$ band in the region of 500 nm and an IVCT band in the near-IR region. The $\pi-\pi^*$ band was observed at a similar wavelength in all the salts (522, 520, and 504 nm in the $TFSI^-$, PF_6^-, and BF_4^- salts, respectively), whereas the IVCT band of the $TFSI^-$ salt appeared in an energy region (1038 nm) lower than that of the PF_6^- and BF_4^- salts (944 and 922 nm, respectively). An intermolecular D−A interaction was

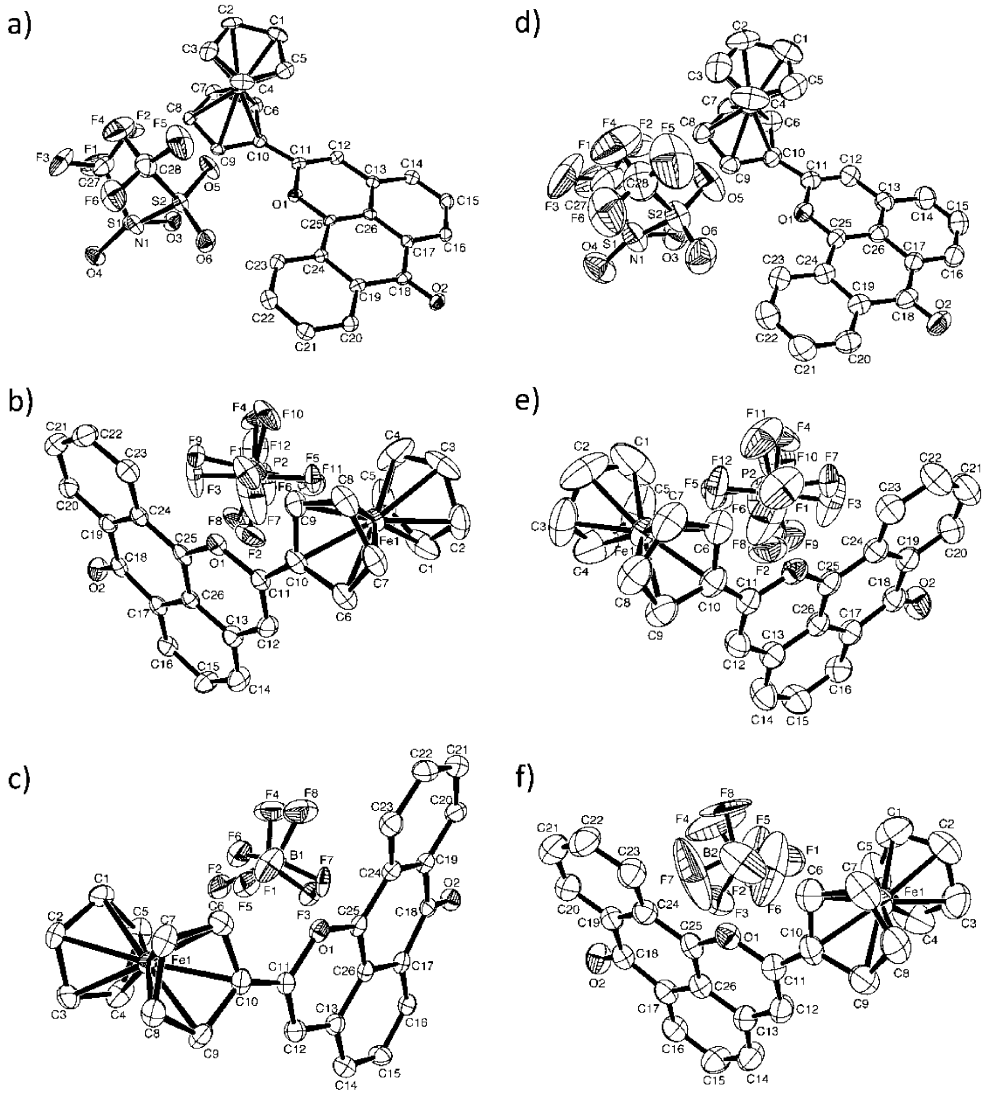

Figure 5. ORTEP plots of **[1-FcPyl]$^+$TFSI$^-$** (a, d), **[1-FcPyl]$^+$PF$_6^-$** (b, e), and **[1-FcPyl]$^+$BF$_4^-$** (c, f) at 113 and 273 K, respectively. Hydrogen atoms are omitted for clarity. Thermal ellipsoids are drawn at the 50% level.

Table 1. Summary of Crystallographic Data of **[1-FcPyl]$^+$X$^-$** (X = TFSI, PF$_6$, or BF$_4$) Measured at 113 and 273 K

	[1-FcPyl]$^+$TFSI$^-$		**[1-FcPyl]$^+$PF$_6^-$**		**[1-FcPyl]$^+$BF$_4^-$**	
empirical formula	$C_{28}H_{17}O_6F_6FeNS_2$		$C_{26}H_{17}O_2F_6FeP$		$C_{26}H_{17}O_2BF_4Fe$	
formula weight	697.4		562.22		504.06	
crystal system	monoclinic		orthorhombic		orthorhombic	
space group	$P2_1/c$		$Pna2_1$		$Pna2_1$	
T (K)	113	273	113	273	113	273
a (Å)	11.463(3)	11.535(3)	21.3928(11)	21.4729(11)	20.936(4)	21.098(3)
b (Å)	10.211(3)	10.241(3)	11.7972(8)	11.9441(8)	11.511(2)	11.6557(18)
c (Å)	23.327(7)	23.567(7)	8.7432(5)	8.7948(5)	8.5179(15)	8.5243(13)
α (deg)	90	90	90	90	90	90
β (deg)	101.0074(14)	101.1257(11)	90	90	90	90
γ (deg)	90	90	90	90	90	90
V (Å^3)	2680.2(13)	2731.5(13)	2206.6(2)	2255.6(2)	2052.8(6)	2096.2(6)
Z	4	4	4	4	4	4
ρ_{calcd} (g·cm^{-1})	1.728	1.696	1.692	1.655	1.631	1.597
μ (cm^{-1})	8.07	7.92	8.31	8.12	7.94	7.77
R1	0.0583	0.0609	0.0387	0.0414	0.0463	0.0437
Rw2	0.1183	0.1498	0.0854	0.0994	0.0924	0.1135
GoF	1.15	1.087	1.057	1.053	1.127	1.091

observed in the crystal structure of the TFSI$^-$ salt (Figure 8); thus, the band in the lowest-energy region could be assigned to the intermolecular charge transfer transition band.[15] The intensity of the IVCT band relative to the $\pi-\pi^*$ band is stronger in the crystalline state than in solution. In the crystalline state, **[1-FcPyl]$^+$** the rotation of the ferrocene moiety was inhibited,

Table 2. Selected Bond Lengths of **[1-FcPyl]$^+$X$^-$** (X = TFSI, PF_6, or BF_4) at 113 and 273 K and **1-FcAq** at 113 K

	[1-FcPyl]$^+$TFSI$^-$		[1-FcPyl]$^+$PF$_6^-$		[1-FcPyl]$^+$BF$_4^-$		1-FcAq
T (K)	113	273	113	273	113	273	113
C(11)−C(12)	1.366(4)	1.362(5)	1.369(4)	1.368(5)	1.369(5)	1.359(5)	1.201(4)
C(17)−C(26)	1.433(4)	1.433(4)	1.428(3)	1.427(4)	1.422(4)	1.421(4)	1.411(3)
C(24)−C(25)	1.447(4)	1.436(4)	1.439(4)	1.439(4)	1.436(5)	1.443(5)	1.494(4)
C(25)−C(26)	1.389(4)	1.389(4)	1.395(4)	1.390(4)	1.395(5)	1.391(4)	1.491(4)
O(1)−C(11)	1.370(3)	1.368(3)	1.355(3)	1.347(4)	1.350(4)	1.344(4)	−
O(1)−C(25)	1.347(3)	1.340(3)	1.335(3)	1.338(3)	1.330(4)	1.332(3)	1.223(3)
O(2)−C(18)	1.231(3)	1.229(4)	1.219(3)	1.224(3)	1.222(4)	1.217(3)	1.221(3)

and the dihedral angle between the donor and acceptor should be small (*vide supra*). In the untwisted structure, the $d_\pi-\pi$ interaction between the ferrocene and pyrylium moieties is strengthened, causing an increase in the intensity of the IVCT band. Therefore, this result indicates that **[1-FcPyl]$^+$** adopts a more planar structure in the crystalline state than in solution.

Variable-Temperature IR Spectroscopy. Data from IR spectra of **[1-FcPyl]$^+$X$^-$** (X = TFSI, PF_6, and BF_4) and **1-FcAq** obtained from a KBr pellet at room temperature are summarized in Table 3. The C≡C bond-stretching vibration at 2208 cm^{-1} in the spectrum of **1-FcAq** was completely absent in the spectrum of **[1-FcPyl]$^+$X$^-$**, which instead contained the vibration of the pyrylium moiety[16] at 1615, 1618, and 1620 cm^{-1} for the TFSI$^-$, PF_6^-, and BF_4^- salts, respectively (Figure S11). All the compounds showed ferrocene vibrations in the region of 460−500 cm^{-1}, assigned to an asymmetric ring−metal−ring tilting vibration and an asymmetric ring−metal−ring stretch. And the vibration of C−H wagging mode of Cp was observed 800−900 cm^{-1} in the TFSI and BF_4 salts. Counterion vibrations were also observed in each salt.

IR spectra of **[1-FcPyl]$^+$X$^-$** (X = TFSI, PF_6, and BF_4) measured at various temperatures are shown in Figures 10, S12, and S13. Although the temperature-dependent spectral change was rather small for each of the salts, an obvious change was observed in the vibrations of the ferrocene moiety. As shown in Figures 10 and 11, the wavenumber of the vibration in the TFSI$^-$ and PF_6^- salts decreased with increasing temperature but was unchanged in the BF_4^- salt. Ferrocenium ion vibrations are usually observed at lower energy than those in ferrocene because the bond strength between the iron and the cyclopentadienyl rings is weaker in ferrocenium ions.[17] Furthermore, the wavenumber of C−H wagging mode drastically changed in the TFSI salt with rising temperature, suggesting the change from the Fe(II) to the Fe (III) state[18] (Figure S12), although the change was not observed in the BF_4 salt. Therefore, the IR results suggest that the valence of the iron in the TFSI$^-$ and PF_6^- salts

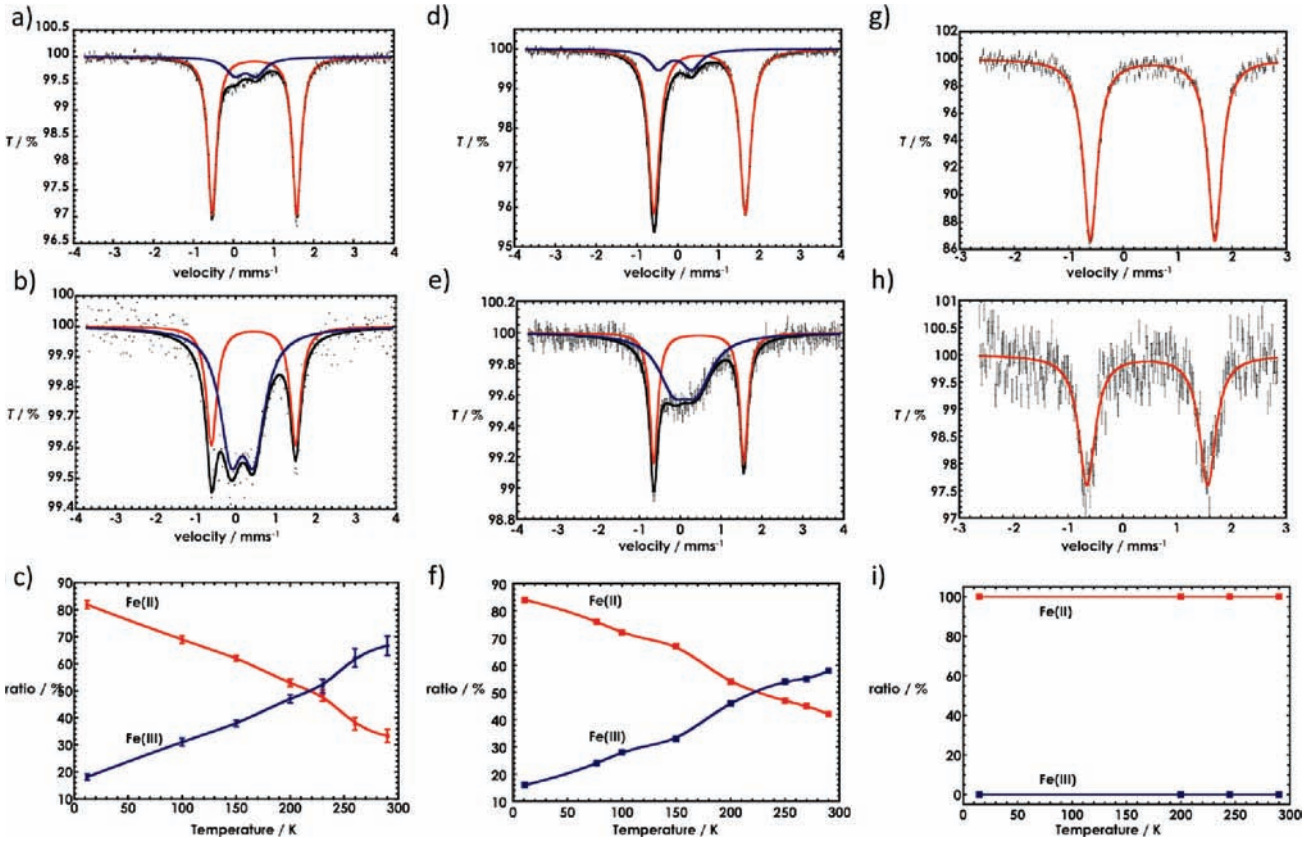

Figure 6. Panels (a), (b), and (c): ^{57}Fe Mössbauer spectra of **[1-FcPyl]$^+$TFSI$^-$** at 12 K, at 290 K, and the change in ϕ^{II} and ϕ^{III} as a function of temperature, respectively. Panels (d), (e), and (f): ^{57}Fe Mössbauer spectra of **[1-FcPyl]$^+$PF$_6^-$** at 11 K, at 290 K, and the change in ϕ^{II} and ϕ^{III} as a function of temperature, respectively. Panels (g), (h), and (i): ^{57}Fe Mössbauer spectra of **[1-FcPyl]$^+$BF$_4^-$** at 15 K, at 295 K, and the change in ϕ^{II} and ϕ^{III} as a function of temperature.

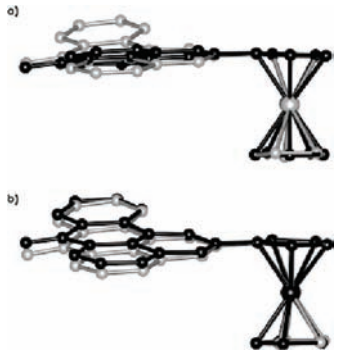

Figure 7. (a) Overlay of crystal structure of **[1-FcPyl]$^+$TFSI$^-$** (black) and **[1-FcPyl]$^+$BF$_4^-$** (gray) and (b) overlay of **[1-FcPyl]$^+$PF$_6^-$** (black) and **[1-FcPyl]$^+$BF$_4^-$** (gray).

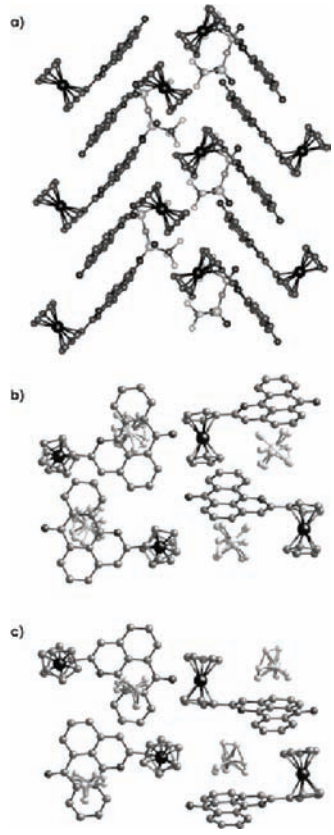

Figure 8. Overall structures of (a) **[1-FcPyl]$^+$TFSI$^-$**, (b) **[1-FcPyl]$^+$PF$_6^-$**, and (c) **[1-FcPyl]$^+$BF$_4^-$**. Hydrogen atoms have been omitted for clarity.

changes from Fe(II) to Fe(III) with increasing temperature, whereas the valence in the BF_4^- salt was unchanged. These conclusions are in agreement with those obtained from the Mössbauer spectra.

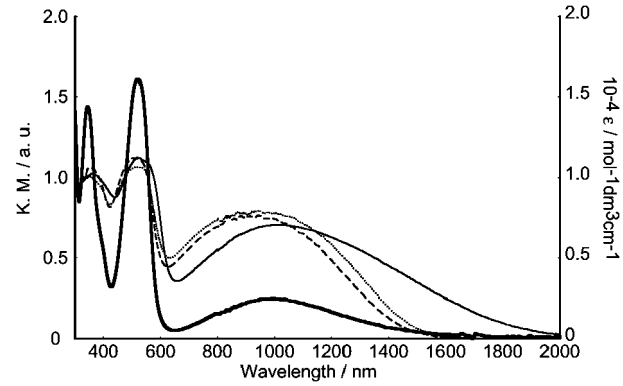

Figure 9. Diffuse reflectance spectra of **[1-FcPyl]$^+$TFSI$^-$** (solid line), **[1-FcPyl]$^+$PF$_6^-$** (dotted line), and **[1-FcPyl]$^+$BF$_4^-$** (dashed line) in the crystalline state (1% in KBr powder), plotted as Kubelka−Munk value (K.M.) on the left-hand axis; and UV−vis−NIR spectrum of 0.5 mM **[1-FcPyl]$^+$TFSI$^-$** (bold solid line) in dichloromethane, plotted as extinction coefficient (ε) on the right-hand axis.

Table 3. Summary of IR Data for **[1-FcPyl]$^+$X$^-$** and **1-FcAq**

compound	C≡C (cm^{-1})	pyrylium (cm^{-1})	counterion (cm^{-1})	Fc (cm^{-1})
[1-FcPyl]$^+$ TFSI$^-$	−	1615	1351, 1328, 1189, 1182, 1160, 1132, 1057, 595, 577, 506	489, 474
[1-FcPyl]$^+$ PF$_6^-$	−	1618	827, 558	494, 476
[1-FcPyl]$^+$ BF$_4^-$	−	1626	1106, 1064, 1037	496, 478
1-FcAq	2217	−	−	492, 473

Structural Change upon Valence Tautomerization. Structural change accompanying VT was studied by single-crystal X-ray analyses. The molecular structures measured at 273 and 113 K are shown in Figure 5d−f. None of the salts showed space group transformation upon change in temperature. The Fe−C(Cp) distances in **[1-FcPyl]$^+$X$^-$** and **1-FcAq** are listed in Table S4; such distances are often used to determine the valence of the ferrocene moiety. The average Fe−C(Cp) distance in **1-FcAq** at 113 K was 2.052(2) Å, which is typical for ferrocene derivatives.[15] The average Fe−C(Cp) distance was 2.048(3) Å in **[1-FcPyl]$^+$TFSI$^-$** at 113 K; this value decreased to 2.037(3) Å at 273 K. However, under the same conditions the average Fe−C(Cp) distance of **[1-FcPyl]$^+$BF$_4^-$** also decreased, from 2.047(2) to 2.039(2) Å, although the BF_4^- salt did not undergo VT. Therefore, the differences in bond length between valence states of the ferrocene moiety were too small to be observed by single-crystal X-ray analyses. Selected bond lengths in **[1-FcPyl]$^+$TFSI$^-$** and **[1-FcPyl]$^+$BF$_4^-$** at 113 and 273 K are shown in Tables 2 and S5. In both salts, the bond lengths of Cp1 (C1−C2−C3−C4−C5) changed slightly with increasing temperature. As shown in Figure 5d−f, the temperature factor of Cp1 becomes larger at 273 K, suggesting that Cp1 rotates freely, preventing accurate determination of the position of carbon atoms in Cp1. Neither salt showed significant temperature-dependent changes in bond length in Cp2 or the acceptor moiety. A difference in bond length between the $TFSI^-$ and BF_4^- salts was not observed, despite the ^{57}Fe Mössbauer spectroscopy results that suggested that ϕ^{III} in the $TFSI^-$ salt increased from 0.3 at 113 K to 0.6 at 273 K. The structural change that accompanies the electron transfer was not observed

(15) (a) Maguères, P. L.; Lindeman, S. V.; Kochi, J. K. *J. Chem. Soc., Perkin Trans. 2* **2001**, 1180–1185. (b) Gouloumis, A.; González-Rodríguez, D.; Vázquez, P.; Torres, T.; Liu, S.; Echegoyen, L.; Ramey, J.; Hug, G. L.; Guldi, D. M. *J. Am. Chem. Soc.* **2006**, *128*, 12674–12684. (c) Small, D.; Zaitsev, V.; Jung, Y.; Rosokha, S. V.; Head-Gordon, M.; Kochi, J. K. *J. Am. Chem. Soc.* **2004**, *126*, 13850–13858. (d) Morimoto, M.; Kobatake, S.; Irie, M. *Chem. Commun.* **2006**, 2656–2658.
(16) Tovar, J. D.; Swager, T. M. *J. Org. Chem.* **1999**, *64*, 6499–6504.
(17) (a) Daggan, D.; Hendrickson, D. N. *Inorg. Chem.* **1975**, *14*, 955, and references therein. (b) Lokshin, B. V.; Aleksankan, V. T.; Rasach, E. B. *J. Organomet. Chem.* **1975**, *86*, 253. (c) Gächter, B. F.; Koningstein, J. A.; Aleksanjan, V. T. *J. Chem. Phys.* **1975**, *62*, 4628.
(18) (a) Berces, A.; Ziegler, T.; Fan, L. *J. Phys. Chem.* **1994**, *98*, 1584–1595. (b) Dai, Y.; Proshlyakov, D. A.; Zak, J. K.; Swain, G. M. *Anal. Chem.* **2007**, *79*, 7526–7533.

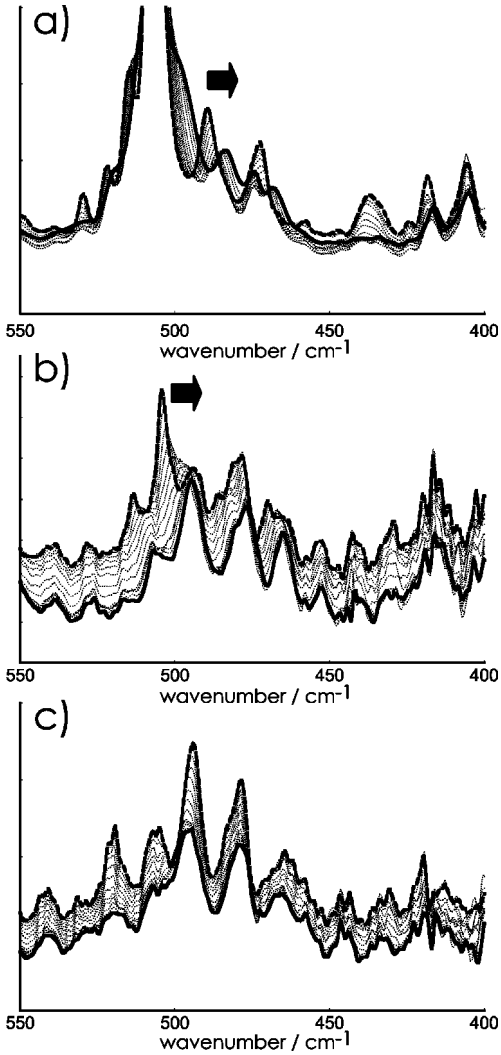

Figure 10. Variable-temperature IR spectra of (a) **[1-FcPyl]$^+$TFSI$^-$**, (b) **[1-FcPyl]$^+$PF$_6^-$**, and (c) **1-FcPyl$^+$BF$_4^-$** in the 400−550 cm^{-1} range. Spectra were measured at various temperatures from 3.5 K (bold dashed line) to 310 K (bold solid line).

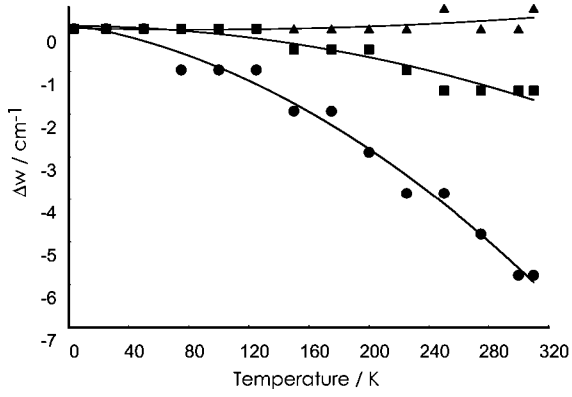

Figure 11. $\Delta w - T$ plots of **[1-FcPyl]$^+$TFSI$^-$** (●), **[1-FcPyl]$^+$PF$_6^-$** (■), and **[1-FcPyl]$^+$BF$_4^-$** (▲). Δw values at each temperature are calculated from the measured wavenumber of the compound by subtracting the wavenumber of the vibration of the ferrocene moiety at 3.5 K.

in the single-crystal X-ray analysis because the π-conjugated system of **[1-FcPyl]$^+$X$^-$** is large, meaning that any changes are spread over a large area of the molecule. The same reasoning applies to the PF$_6^-$ salt.

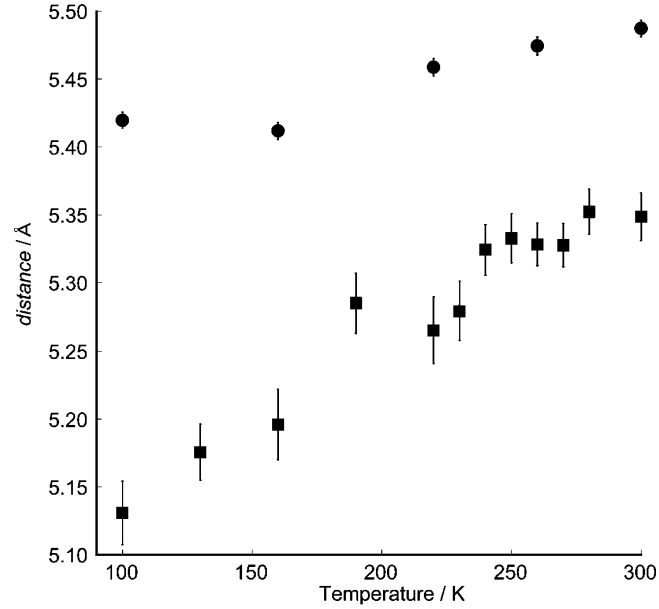

Figure 12. Changes in Fe−P distance in **[1-FcPyl]$^+$PF$_6^-$** (circles) and Fe−B distance in **[1-FcPyl]$^+$BF$_4^-$** (squares) with temperature.

XRPD Measurements and Restrained Rietveld Analysis. Restrained Rietveld analysis of the variable-temperature XRPD data was used to study in detail the effects of the various anions. Synchrotron XRPD measurements were performed at SPring-8 BL02B2, and patterns were collected from 100 to 300 K. The structures of the **[1-FcPyl]$^+$** moiety in the BF$_4^-$ and PF$_6^-$ salts were consistent with those observed in the single-crystal X-ray analysis, and significant temperature-dependent changes in bond length were not observed.

We focused on the distance between the central B or P atom in the anion and the Fe in the ferrocene moiety, as this distance should be dependent on the electronic structure of the complex. Figure 12 shows the dependence of the Fe−B and Fe−P distances on temperature from 100 to 300 K. The distinct difference between the two salts is that the Fe−B distance increased gradually with increasing temperature, whereas the Fe−P distance did not. This difference reflects the fact that VT occurs in the PF$_6^-$ salt but not in the BF$_4^-$ salt. The changes in the Fe−B distance in the BF$_4^-$ salt could be utilized as an indicator of a normal complex that does not undergo VT. The Fe−B distance increases at higher temperatures, as thermal vibration causes expansion of the cell and an increase in intermolecular distances. In contrast, the PF$_6^-$ salt did not exhibit significant temperature-dependent changes in distance due to the occurrence of VT: the molar ratio of the Fe(III) species increases, resulting in increased Coulombic force between the ferrocene moiety and the PF$_6^-$ anion, thereby preventing any increase in Fe−P distance. In the case of the BF$_4^-$ salt, single-crystal X-ray analysis indicated that the dihedral angle between the ferrocene and the pyrylium moiety was the largest among the three salts, resulting in a weaker D−A interaction and low stability of the Fe(III) species (*vide supra*).

Magnetic Susceptibility Measurements. To determine the spin state of the Fe(III) species, magnetic susceptibility measurements were performed on **[1-FcPyl]$^+$X$^-$** (X = TFSI, PF$_6$, and BF$_4$). The magnetic susceptibility of each salt was close to zero from 5 to 400 K (Figure S14). ^{57}Fe Mössbauer spectroscopy showed the BF$_4^-$ salt to be in the diamagnetic Fe(II) state in this temperature range, accounting for its diamagnetic magnetization

behavior. In the case of the $TFSI^-$ and PF_6^- salts, ^{57}Fe Mössbauer spectroscopy indicated the presence of the Fe(III) species possessing two electronic spins, yet paramagnetic susceptibility was not observed. Therefore, we conclude that the electronic spins are antiferromagnetically coupled in these two salts. Although the crystal structures of the $TFSI^-$ salt and PF_6^- salt are significantly different, the magnetic properties of both salts were approximately the same. This finding suggests that the organic radical and the ferrocenium ion are antiferromagnetically coupled intramolecularly, not intermolecularly.

Discussion

The mechanism of VT phenomena of **[1-FcPyl]**$^+$ salts is discussed in this section. It is revealed from various experiments that crystals of **[1-FcPyl]**$^+$**TFSI**$^-$ and **[1-FcPyl]**$^+$**PF$_6^-$** exhibit VT phenomena, although crystals of **[1-FcPyl]**$^+$**BF$_4^-$** and all salts in the solution phase do not.

As mentioned above, in the solution state, the difference of the redox potentials of donor and acceptor is relatively large because of their weak electronic interaction. In solution, the free rotation of Fc against Pyl^+ is expected to occur. The results of TD-DFT calculation indicate that the large ϕ_1 causes the large HOMO−LUMO gap as shown in Figure S10. Therefore, it is concluded that the free rotation prevents the electron transfer from donor to acceptor, and thus VT phenomena was not observed in solution.

In contrast, the free rotation is completely inhibited in the crystalline state. D'Avino et al.[7b] reported the example of VT phenomena that caused by the change of dipole moment arising from electron transfer. However, in our case, the change of dipole moment accompanied by charge transfer is relatively small because both Fe(II) and Fe(III) states are cationic species. This tendency was confirmed by the small solvatochromic behavior of **[1-FcPyl]**$^+$ in solution. Furthermore, the intermolecular interaction between **[1-FcPyl]**$^+$s does not play any dominant role on the VT phenomena because both the TFSI salt with the intermolecular interaction and the PF_6 salt without the interaction exhibited VT phenomena in the crystalline state. Therefore, we focused on the conformational change of the **[1-FcPyl]**$^+$ and the interaction of the complex cation with counteranion in the three salts.

All the salts have similar conformation as shown in Figure 7, but the rotation of the donor moiety (ϕ_1) and the distortion of the acceptor moiety (ϕ_2) of the BF_4 salt were bigger than those of other two salts (for details, see above). The large ϕ_1 causes the expansion of the HOMO−LUMO gap, and the large ϕ_2 destabilizes the acceptor moiety and raises the LUMO energy. These two structural distortions inhibit the electron transfer.

Different temperature dependency of the distance between the central B or P atom in the anion and the Fe in the ferrocene moiety was observed between the BF_4^- and PF_6^- salts (for details, see above). We have concluded that the small temperature dependency of the distance in the PF_6^- salt is related to the VT phenomenon. Instead, the electrostatic interaction of the **[1-FcPyl]**$^+$ moiety with PF_6^- that is stronger than that with BF_4^- may be a cause of the occurrence of VT. It is noteworthy that VT without significant structural change has been reported for a biferrocenium(1^+) salt;[19] furthermore, interaction between the cation and the anion played a key role in the temperature-dependent VT.

Moreover, results of ^{57}Fe Mössbauer measurement indicate that the relative population of two species is not governed by the Boltzmann equation in the TFSI salt. In other words, **1-Fc$^+$Pyl** species are stabilized in higher temperature region. We could not find the exact reason for this phenomenon, but the flat configuration and/or strong electrostatic interaction with $TFSI^-$ might affect the stability of the **1-Fc$^+$Pyl** speices.

Conclusion

The nature of the anion in **[1-FcPyl]**$^+$**X**$^-$ salts (X = TFSI, TfO, BF_4, and PF_6) strongly affected the occurrence of VT between **1-FcPyl**$^+$ and **1-Fc$^+$Pyl** in the solid state. ^{57}Fe Mössbauer spectroscopy (11−300 K) indicated that the $TFSI^-$ and PF_6^- salts exhibited VT in the solid state, but the BF_4^- salt did not. The structural change upon electron transfer was observed by variable-temperature IR spectroscopy. In this measurement, the frequencies of skeletal vibration of the ferrocene moiety decreased with increasing temperature in the $TFSI^-$ and PF_6^- salts, indicating the development of ferrocenium-like character. The larger ϕ_1 in the BF_4^- salt (11.23(15)°) compared with the $TFSI^-$ (6.63(12)°) and PF_6^- (9.55(12)°) salts suggested a weaker D−A interaction, and therefore lower stability of the Fe(III) species in the BF_4^- salt. Furthermore, the more distorted acceptor moiety in the BF_4 salts caused the higher LUMO energy. VT-XRPD measurement also suggested the structural change upon electron transfer process. We found that the differences in the interaction of **1-FcPyl**$^+$ with the PF_6^- and BF_4^- ions were revealed by the temperature dependence of the Fe−P and Fe−B distances, respectively. The Fe−P bond length in the PF_6^- salt exhibited smaller temperature dependence than the Fe−B bond length in the BF_4^- salt because the Coulombic interaction between Fe and P prevents thermal movement of counteranions. These results were consistent with a temperature-dependent increase in the Fe(III) species in the PF_6^- salt.

In conclusion, we have found that the VT phenomena of **[1-FcPyl]**$^+$ salts are controlled by the small difference of the dihedral angle between the ferrocene and the pyrylium moieties and of the distortion of the acceptor moiety and/or the magnitude of electrostatic interaction of the complex cation with the counteranion.

Experimental Section

General Method. Solvents and reagents were used as received from commercial sources unless noted otherwise. Ethynylferrocene was prepared by a procedure described in the literature.[20] Anhydrous solvents were obtained as Guaranteed grade from Kanto Chemicals Ltd. and used after a freeze−pump−thaw unless noted otherwise. Triethylamine was dried by reflux over KOH, distilled under nitrogen, and degassed with a freeze−pump−thaw. Hexane, dichloromethane, and 1,2-dichloroethane were distilled from CaH_2 under nitrogen, and degassed with a freeze−pump−thaw. All syntheses were performed under an atmosphere of dry nitrogen or dry argon unless otherwise indicated.

NMR Measurements and Mass Spectrometry. ^1H and ^{13}C NMR spectra and HMQC of samples in chloroform-d_1 and acetonitrile-d_3 were collected with an AL-400 (JEOL), ECX400 (JEOL), or DRX500 NMR spectrometer (Bruker). MALDI-TOF and ESI-TOF mass spectra were recorded with a AXIMA-CFR spectrometer (Shimadzu Kratos) and an LCT time-of-flight mass spectrometer (Micromass), respectively.

(19) Mochida, T.; Takazawa, K.; Matsui, H.; Takahashi, M.; Takeda, M.; Sato, M.; Nishio, Y.; Kajita, K.; Mori, H. *Inorg. Chem.* **2005**, *44*, 8628–8641.

(20) Rosenblum, M.; Brawn, N.; Papenmeir, J.; Applebaum, M. *J. Organomet. Chem.* **1966**, *6*, 173–180.

Single-Crystal X-ray Structural Analysis. The crystals were mounted in a loop. Data were collected using an AFC8 diffractometer with a Mercury CCD system equipped with a rotating-anode X-ray generator (Rigaku). The employed X-rays were graphite-monochromated Mo Kα radiation ($\lambda = 0.7107$ Å). An empirical absorption correction using equivalent reflections and Lorentzian polarization was performed with the program Crystal Clear 1.3.5. The structure was solved with the program SHELXS-97[21] and refined against F^2 using SHELXL-97.[22]

XRPD Measurements and Restrained Rietveld Analysis. The powder samples were sealed in glass capillaries (0.4 mm internal diameter) for X-ray analysis. The synchrotron radiation powder diffraction experiments were carried out at the SPring-8, BL02B2 beamline.[23] A two-dimensional imaging plate detector was used to achieve high counting statistics. The temperature of the sample was controlled using a low-temperature N_2 gas flow apparatus. The wavelengths of the incident X-rays were 0.80152(5) Å and 0.80178(5) Å for **[1-FcPyl]$^+$BF$_4^-$** and **[1-FcPyl]$^+$PF$_6^-$**, respectively. Total exposure time was 15 min. The X-ray powder diffraction patterns were obtained in 0.01° steps of 2θ from 2.3° to 60.0° for **[1-FcPyl]$^+$BF$_4^-$** and **[1-FcPyl]$^+$PF$_6^-$**. Both patterns correspond to 0.802 Å resolution in *d*-spacing. Restrained Rietveld refinements were carried out using the refinement program Synchrotron-Powder (SP).[24]

UV−vis−near-IR Spectroscopy in Solution. Samples for UV−vis−near-IR spectroscopy in solution were prepared under an argon atmosphere. UV−vis−NIR spectra were recorded with a V-570 spectrometer (JASCO). Quartz cells with a path length of 0.1 cm were utilized to observe absorption in the UV region.

Diffuse Reflectance UV−vis−NIR Spectroscopy. Diffuse reflectance UV−vis−NIR spectra were recorded with a JASCO V-570 spectrometer equipped with an integrated sphere. The baseline was measured using KBr powder. Samples were prepared from compound powder dispersed in KBr (1%). Microcrystals of KBr were ground with an agate pestle and mortar, compound powder was added, and KBr and compound were mixed gently to homogeneity before packing in the cell.

Variable-Temperature IR Spectroscopy. IR spectra were recorded at various temperatures from 3.5 to 310 K with a JASCO FT/IT-620 V spectrometer equipped with a liquid-He cryostat. All spectra was measured as KBr pellets, which were fabricated in a similar manner as described above for the diffuse reflectance UV−vis−NIR spectroscopy.

Magnetic Susceptibility Measurement. Magnetic measurements were carried out using an MPMS-5S superconducting quantum interference device spectrometer (SQUID) at a field length of 1 T (Quantum Design). Samples for magnetic susceptibility measurements were prepared as follows. Microcrystals of compound under an argon atmosphere were wrapped with aluminum foil sized ca. 15 mm × 15 mm, and the sample size was adjusted to ca. 6 mm × 6 mm. The sample was fixed in a plastic straw having projections for use as a stopper. The paramagnetic susceptibility of each sample was calculated by subtraction of the value obtained for aluminum foil alone.

DFT Calculation. DFTs were calculated using the three-parametrized Becke−Lee−Yang−Parr (B3LYP) hybrid exchange-correlation functional. The geometry of **[1-FcPyl]$^+$** was optimized by the DFT(B3LYP) method without accounting for solvent effects, using the crystal structure as the initial value and the Lanl2DZ (Hay−Wadt ECP) basis set for all atoms. Transition energy and oscillator strength were calculated by the TD-DFT method without accounting for solvent effects. Series of calculations were carried out using Gaussian 03 (revision B.05) or Gaussian 03W (revision B.05).[25]

^{57}Fe Mössbauer Spectroscopy. The ^{57}Fe Mössbauer spectra of **[1-FcPyl]$^+$X$^-$** were measured with a Wissel MVT-1000 Mössbauer Transducer equipped with an MDU-1200 Function Generator and Driving Unit and a Reuter-Stokes RS-P3-1605-262 proportional γ-ray counter against 925 MBq of ^{57}Co/Rh at temperatures ranging from 12 to 290 K.

Synthesis of 2-Ferrocenyl-7-oxo-7,11b-dihydrodibenzo[*de*,*h*]chromenylium Bis(trifluoromethylsulfonyl)amide. ([1-FcPyl]$^+$-TFSI$^-$). 1-Ferrocenylethynylanthraquinone (102 mg, 0.245 mmol) was dissolved in 10 mL of dichloromethane under an argon atmosphere. Bis(trifluoromethanesulfone)imide (116 mg, 0.411 mmol) was added to the stirred solution, resulting in an immediate color change from red to dark red, and the solution was stirred for a further 10 min. Red crystals were collected by filtration. Yield: 140.0 mg (82%). ^{1}H NMR (400 MHz, CD_3CN): δ (ppm) 4.35 (s, 5H, Cp), 5.06 (t, $J = 1.5$ Hz, 2H, Cp), 5.41 (t, $J = 1.5$ Hz, 2H, Cp), 8.10 (m, 2H, fused ring (FR)), 8.19 (d, $J = 8.3$ Hz, 1H, FR), 8.23 (s, 1H, FR), 8.36 (m, 1H, FR), 8.46 (m, 1H, FR), 8.58 (d, $J = 8.3$ Hz, 1H, FR), 8.69 (m, 1H, FR). ^{13}C NMR (100 MHz, CD_3CN): δ (ppm) 69.9 (Cp), 72.7 (Cp), 73.4 (Cp), 76.1 (Cp), 116.5 (FR), 119.2 (CF_3), 120.9 (FR), 122.3 (CF_3), 127.9 (FR), 129.0 (FR), 130.1 (FR), 130.5 (FR), 133.8 (FR), 134.2 (FR), 134.9 (FR), 136.6 (FR), 137.8 (FR), 141.5 (FR), 142.1 (FR), 167.7 (FR), 170.9 (FR), 180.6 (FR). Anal. Calcd. for $C_{28}H_{17}O_6F_6FeNS_2$: C, 48.22; H, 2.46; N, 2.01. Found: C, 48.18; H, 2.70; N, 2.22.

Synthesis of 2-Ferrocenyl-7-oxo-7,11b-dihydrodibenzo[*de*,*h*]chromenylium Triflate. ([1-FcPyl]$^+$TfO$^-$). Compound **1-FcAq** (60 mg, 0.14 mmol) was dissolved in 20 mL of dichloromethane under an argon atmosphere. Trifluoromethanesulfonic acid (40 μL, 0.45 mmol) was added to the stirred solution, stirring was continued for a further 10 min, and hexane (40 mL) was added. Deep red crystals were collected by filtration. Yield: 75 mg (95%). ^{1}H NMR (400 MHz, CD_3CN): δ (ppm) 4.35 (s, 5H, Cp), 5.06 (t, $J = 1.8$ Hz, 2H, Cp), 5.40 (t, $J = 1.8$ Hz, 2H, Cp), 8.09 (m, 2H, fused ring (FR)), 8.20 (d, $J = 8.0$ Hz, 1H, FR), 8.23 (s, 1H, FR), 8.35 (m, 1H, FR), 8.46 (m, 1H, FR), 8.58 (d, $J = 8.0$ Hz, 1H, FR), 8.69 (m, 1H, FR).

Synthesis of 2-Ferrocenyl-7-oxo-7,11b-dihydrodibenzo[*de*,*h*]chromenylium Tetrafluoroborate. ([1-FcPyl]$^+$BF$_4^-$). Compound **[1-FcPyl]$^+$TfO$^-$** (22 mg, 0.038 mmol) was dissolved in 20 mL of dichloromethane under an argon atmosphere. Tetra(*n*-butylammonium)tetrafluoroborate (15 mg, 0.046 mmol) was added to the stirred solution, and stirring was continued for a further 20 min. Red crystals were collected by filtration. Yield: 8.4 mg (43%). ^{1}H NMR (400 MHz, CD_3CN): δ (ppm) 4.35 (s, 5H, Cp), 5.06 (t, $J = 1.8$ Hz, 2H, Cp), 5.40 (t, $J = 1.8$ Hz, 2H, Cp), 8.09 (m, 2H, fused ring (FR)), 8.20 (d, $J = 8.0$ Hz, 1H, FR), 8.23 (s, 1H, FR), 8.35 (m, 1H, FR), 8.46 (m, 1H, FR), 8.58 (d, $J = 8.0$ Hz, 1H, FR), 8.69 (m, 1H, FR). Anal. Calcd for $C_{26}H_{17}O_6F_4FeB$: C, 61.95; H, 3.40. Found: C, 61.99; H, 3.71.

Synthesis of 2-Ferrocenyl-7-oxo-7,11b-dihydrodibenzo[*de*,*h*]chromenylium Hexafluorophosphate. ([1-FcPyl]$^+$PF$_6^-$). Compound **[1-FcPyl]$^+$TfO$^-$** (21 mg, 0.037 mmol) was dissolved in 20 mL of dichloromethane under an argon atmosphere. Tetra(*n*-butylammonium)hexafluorophosphate (24 mg, 0.061 mmol) was added to the stirred solution, and stirring was continued for a further 20 min. Deep-purple crystals were collected by filtration. Yield: 10.1 mg (49%). ^{1}H NMR (400 MHz, CD_3CN): δ (ppm) 4.35 (s, 5H, Cp), 5.06 (t, $J = 1.8$ Hz, 2H, Cp), 5.40 (t, $J = 1.8$ Hz, 2H, Cp), 8.09 (m, 2H, fused ring (FR)), 8.20 (d, $J = 8.0$ Hz, 1H, FR), 8.23 (s, 1H, FR), 8.35 (m, 1H, FR), 8.46 (m, 1H, FR), 8.58 (d, J

(21) Sheldrick, G. M. *Program for Crystal Structure Solution*; University of Gottingen: Germany, 1997.
(22) Sheldrick, G. M. *Program for Crystal Structure Refinement*; University of Gottingen: Germany, 1997.
(23) Nishibori, E.; Takata, M.; Kato, K.; Sakata, M.; Kubota, Y.; Aoyagi, S.; Kuroiwa, Y.; Yamakata, M.; Ikeda, N. *Nucl. Instrum. Methods* **2001**, *A467*, 1045–1048.
(24) Nishibori, E.; Sunaoshi, E.; Yoshida, A.; Aoyagi, S.; Kato, K.; Takata, M.; Sakata, M. *Acta Crystallogr.* **2007**, *A63*, 43–52.
(25) Frisch, M. J.; et al. *Gaussian 03*, revision-B.05; Gaussian, Inc.: Pittsburgh, PA, 2003. (For complete author list, see Supporting Information.)

= 8.0 Hz, 1H, FR), 8.69 (m, 1H, FR). Anal. Calcd for $C_{26}H_{17}O_6F_6FeP$: C, 55.44; H, 3.05. Found: C, 55.39; H, 3.25.

Acknowledgment. This work was supported by Grants-in-Aid for Scientific Research (Nos. 18655021 and 20245013) from MEXT, Japan, and by a Research Fellowship from the Japan Society for the Promotion of Science for Young Scientists.

Supporting Information Available: Crystallographic information files (CIF) of **[1-FcPyl]$^+$X$^-$** and extensive figures and tables; complete ref . This material is available free of charge via the Internet at http://pubs.acs.org.

JA900393E